ACS APPLIED NANO MATERIALS
Cite This: ACS Appl. Nano Mater. 2019, 2, 6022−6029
Article
www.acsanm.org

Understanding Reduced CO_2 Uptake of Ionic Liquid/Metal−Organic Framework (IL/MOF) Composites

Xiaoxiao Xia,[†,‡] Guoqing Hu,[†,‡] Wei Li,[†,‡] and Song Li*[,†,‡,§]

[†]State Key Laboratory of Coal Combustion, School of Energy and Power Engineering, Huazhong University of Science and Technology, Wuhan 430074, China

[‡]Nano Interface Center for Energy, School of Energy and Power Engineering, Huazhong University of Science and Technology, Wuhan 430074, China

[§]China-EU Institute for Clean and Renewable Energy, Huazhong University of Science and Technology, Wuhan 430074, China

Supporting Information

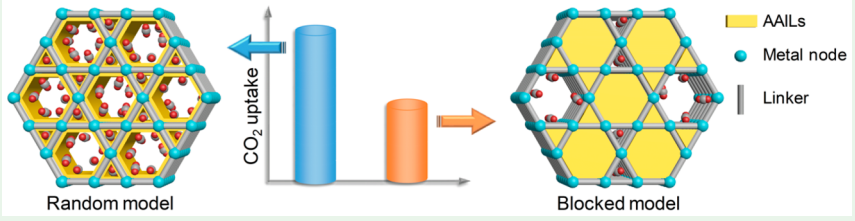

ABSTRACT: Reduced CO_2 uptake of ionic liquid/metal−organic framework (IL/MOF) composites has been observed in many experiments. However, simulation study gives rise to the opposite tendency. To understand such a phenomenon, both experiment and simulation were performed in this work. Two amino acid ionic liquids (AAILs) (i.e., [Emim][Gly] and [Emim][Phe]) and two Zr-based MOFs (i.e., UiO-66 and NU-1000) were used to prepare a variety of IL/MOF composites. The reduced CO_2 uptake observed in all IL/MOF composites upon ILs loading regardless of the amount of ILs is consistent with previous experimental reports. According to pore size distribution, similar pore sizes of the composites to those of pristine MOFs revealed that the blocking of channels by loaded AAILs into MOFs occurred, leading to decreased uptakes. Moreover, molecular simulation demonstrated that the blockage in channels significantly decreased CO_2 uptake compared with the model consisting of randomly distributed ILs, which approximates experimental observations. This study provides experimental and theoretical evidence for the existing blockage in MOF channels upon ILs introduction, which contributed to the reduced CO_2 uptakes of IL/MOF composites.

KEYWORDS: *amino acid ionic liquids, metal−organic frameworks, composites, CO_2 adsorption, blockage*

1. INTRODUCTION

Metal−organic frameworks (MOFs)[1] have been identified as promising adsorbents for carbon dioxide (CO_2) capture[2,3] due to their high surface area, structure tunability, and facile synthesis. In recent decades, postsynthetic modification of MOFs[4] including chemical functionalization and functional molecules impregnation has been adopted to further enhance their CO_2 adsorption performance. Due to the complicated manipulation of chemical functionalization, physical modification by introducing functional molecules into frameworks that exhibit high affinity toward CO_2 is a promising alternative. Recent studies have concentrated on improving CO_2 adsorption performance of MOFs by introducing ionic liquids (ILs)[5] into the porous frameworks.[6] Many simulation studies have showed that IL/MOF composites display the higher affinity toward CO_2 molecules than pristine MOFs. Chen et al.[7] reported the 1-butyl-3-methylimidazolium hexafluorophosphate ([Bmim][PF_6])/IRMOF-1 composites are more promising CO_2 adsorbents by molecular simulations, in which the introduction of [Bmim][PF_6] not only enhanced the CO_2/N_2 selectivity but also significantly increased CO_2 adsorption capacity at 1 bar due to the increased ionic adsorption sites provided by [Bmim][PF_6]. However, the high weight percentage of ILs may decrease the CO_2 uptake due to the reduced adsorption sites within frameworks by additional ILs. Vicent-Luna et al.[8] reported that both CO_2/N_2 and CO_2/CH_4 selectivities were increased by incorporating five types of ILs (i.e., [Emim][SCN], [Emim][Tf_2N], [Emim][BF_4], [Emim][NO_3], and [Emim][PF_6]) into Cu-BTC, respectively, by simulation. Simultaneously, their CO_2 uptakes were also significantly enhanced within 1 bar after loading ILs (8 molecules per unit cell) regardless of ILs type.[8] Except for CO_2 uptakes, molecular simulation demonstrated that introducing [Bmim][Cl] can also significantly enhance H_2S uptake at low ILs loadings compared to pristine Cu-TDPAT.[9]

Received: August 13, 2019
Accepted: August 20, 2019
Published: August 20, 2019

DOI: 10.1021/acsanm.9b01538
ACS Appl. Nano Mater. 2019, 2, 6022−6029

However, such an enhancement on CO_2 uptake upon introducing ILs within 1 bar has seldom been reported in experimental studies. On the contrary, the reduced CO_2 adsorption of IL/MOF composites has been frequently observed. The decreased CO_2 uptake in IL/Cu-BTC composites compared with bare Cu-BTC observed in experiments has been ascribed to the disrupted porous network of Cu-BTC after the impregnation of ILs.[10] The CO_2, CH_4, N_2, and H_2 adsorption performance of Cu-BTC with impregnated 1-butyl-3-methylimidazolium tetrafluoroborate ([Bmim][BF_4]) has also been investigated.[11] Compared to pristine Cu-BTC, not only CO_2 but also the other gas adsorption capacities of [Bmim][BF_4]/Cu-BTC composites were reduced. Nevertheless, CO_2/H_2, CH_4/H_2, CH_4/N_2, and N_2/H_2 selectivities of [Bmim][BF_4]/Cu-BTC composites have been obviously improved at low pressures (i.e., 0.1−1 bar). The decreased CO_2 uptake at 1 bar was also reported for task-specific ionic liquid (i.e., [C_3NH_2BIM][Tf_2N])/NH_2-MIL-101(Cr)[12] and IL/ZIF-8 composites without disrupting frameworks.[13−15] Although the improved CO_2 uptake at ultralow pressure (below 1 bar) has been experimentally demonstrated for [Bmim][Tf_2N]/ZIF-8,[13] [Bmim][PF_6]/ZIF-8,[14] and [Bmim][BF_4]/ZIF-8[15] regardless of the amount of loaded ILs, their CO_2 uptakes at 1 bar were evidently lower than pristine ZIF-8. So far, the improved gas selectivity of IL/MOF composites has been consistently verified by both experimental measurements and molecular simulations. However, the opposite trend in CO_2 uptake of IL/MOF composites at 1 bar between molecular simulations and experiments has been frequently reported.

In order to understand the inconsistent CO_2 uptake between experiments and simulations, we performed systematic studies on the CO_2 adsorption performance of varying IL/MOF composites by both experiments and molecular simulations. Two Zr-based MOFs, i.e., UiO-66 and NU-1000, were chosen because of their good thermal and chemical stability.[16] Environment-friendly amino acids ionic liquids (AAILs) were chosen because of their known high affinity toward CO_2 in the presence of $-NH_2$ groups in the structures.[17] Herein, two AAILs, 1-ethyl-3-methylimidazolium glycinate ([Emim][Gly]) and 1-ethyl-3-methylimidazolium phenylalanate ([Emim][Phe]), were incorporated into two types of MOFs at different loadings (5, 10, and 30 vol %) according to the total pore volume of MOFs. Both experimental and molecular simulation were implemented to disclose the mechanism of the reduced CO_2 uptake in IL/MOF composites.

2. RESULTS AND DISCUSSION

According to the total pore volume of UiO-66 and NU-1000 (Table S1), 5, 10, and 30 vol % AAILs (Table S2) were used for AAIL/MOF composites preparation. The consistency in powder X-ray diffraction (PXRD) patterns of pristine MOFs and their AAIL/MOF composites (Figure 1a,b and Figure S3) demonstrates that AAILs loading did not disrupt the MOF frameworks, similar to a previous report.[11] Similarly, a previous report on 1-ethyl-3-methylimidazolium bis(trifluoromethylsulfonyl)amide ([Emim][TFSA])/ZIF-8 composites[18] also showed the decreased PXRD intensity of ZIF-8 upon ILs loading. Scanning electron microscopy (SEM) images showed that the morphology of MOFs was almost not altered after AAILs loading (Figure 1c−f). Thermal gravimetric analysis (TGA) of AAIL/UiO-66 (Figure S6) and AAIL/NU-1000 composites (Figure S7) demonstrates the high thermal stability

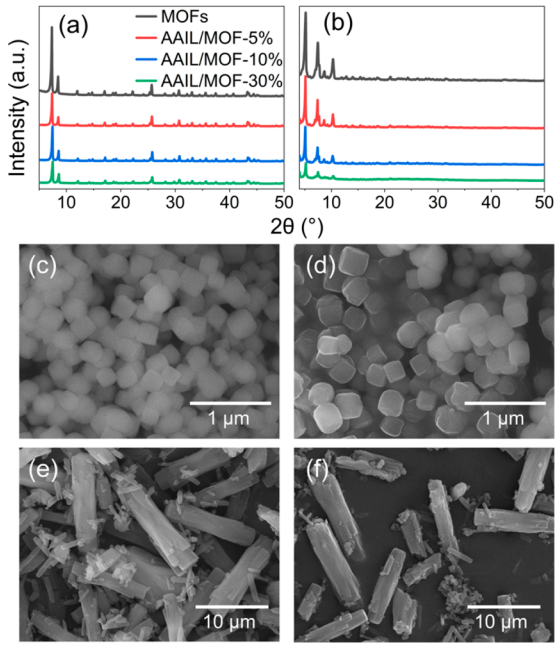

Figure 1. PXRD of (a) [Emim][Gly]/UiO-66 and (b) [Emim][Gly]/NU-1000 composites. SEM images of (c) UiO-66, (d) [Emim][Gly]/UiO-66-30%, (e) NU-1000, and (f) [Emim][Gly]/NU-1000-30%.

of AAIL/MOF composites. Brunauer−Emmett−Teller (BET) surface area and total pore volume of [Emim][Gly]/MOF (Table 1) are decreased with the loading of AAILs, in

Table 1. BET Surface Area and Total Pore Volume of MOFs and [Emim][Gly]/MOF Composites

sample	BET surface area (m^2/g)	total pore volume (cm^3/g)
UiO-66	1508	0.987
[Emim][Gly]/UiO-66-5%	1102	0.736
[Emim][Gly]/UiO-66-10%	861	0.620
[Emim][Gly]/UiO-66-30%	331	0.514
NU-1000	2362	1.491
[Emim][Gly]/NU-1000-5%	1754	1.118
[Emim][Gly]/NU-1000-10%	1378	0.902
[Emim][Gly]/NU-1000-30%	265	0.180

agreement with the previous study,[11] in which ILs loading reduces both BET surface area and pore volume of MOFs. A similar trend has also been found in [Emim][Phe]/UiO-66 (Table S3) and [Emim][Phe]/NU-1000 (Table S4).

As expected, the reduced CO_2 uptake compared with pristine MOFs was observed in adsorption isotherms of both [Emim][Gly]/MOF and [Emim][Phe]/MOF composites (Figure 2) regardless of the amount of loaded AAILs, which was decreased with the increased loading of AAILs. Such a tendency is opposite to previous simulation studies[7,8] but consistent with reported experimental observations in IL/Cu-BTC,[11] IL/NH_2-MIL-101,[12] IL/ZIF-8,[13−15] and so on. The reduced CO_2 uptake may be ascribed to the presence of multiple blocked pores in frameworks during ILs introduction, which prevents the entrance of additional ILs and thus is unfavorable for the uniform distribution of ILs on pore surfaces, leading to decreased number of adsorption sites. However, so far, there is no direct evidence of such a possibility. To further interpret such a phenomenon, we

DOI: 10.1021/acsanm.9b01538
ACS Appl. Nano Mater. 2019, 2, 6022−6029

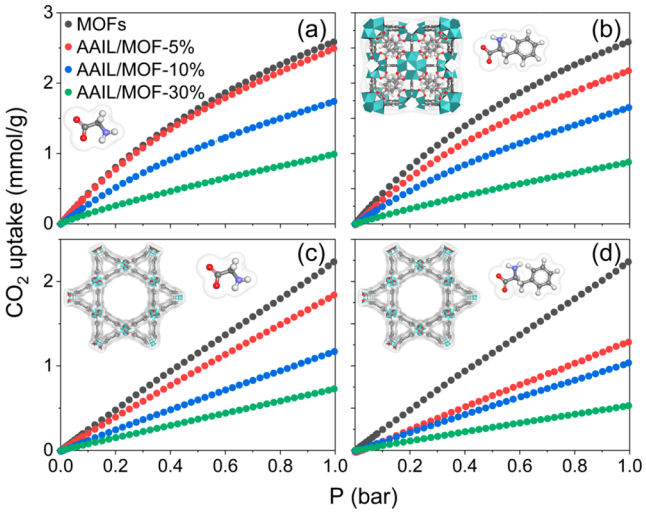

Figure 2. CO_2 adsorption isotherms of (a) [Emim][Gly]/UiO-66, (b) [Emim][Phe]/UiO-66, (c) [Emim][Gly]/NU-1000, and (d) [Emim][Phe]/NU-1000.

analyzed the pore size distributions (PSDs) of AAIL/MOF composites (Figure 3), in which there is no obvious change in pore sizes of both [Emim][Gly]/UiO-66 and [Emim][Gly]/NU-1000 upon AAILs loading, whereas the peak intensity of PSD decreased with the increase of [Emim][Gly] loading, indicating the reduced pore volumes resulting from the occupied space of [Emim][Gly]. At 30 vol % loadings, the vast majority of pore space of MOFs was occupied by AAILs, especially for [Emim][Gly]/NU-1000 and [Emim][Phe]/NU-1000, resulting in low CO_2 uptake.

Given the identical pore widths of bare MOFs and AAIL/MOFs composites, the partially blocked pore channels of MOF frameworks can be extrapolated (Figure 3e–g). Instead of uniform distribution on the channel surface, AAILs are highly accumulated in channels, most probably in pore windows, thus leading to identical pore sizes of MOFs and AAIL/MOF composites in PSDs and the decreased pore volume with AAILs introduction. In practice, there are numerous possibilities for the distribution and locations of blockage in channels. To simplify this issue and to further understand such a tendency, molecular dynamics (MD) and grand canonical Monte Carlo (GCMC) simulations were performed using [Emim][Gly]/NU-1000 as an example. Moreover, in order to elucidate the origin of the opposite trends in CO_2 uptake of IL/MOF composites from experimental measurements and simulations that has been frequently observed, two different [Emim][Gly]/NU-1000 models, i.e., random and blocked models, were adopted. Regarding random models (Figure 4a–c), AAILs are randomly inserted into frameworks, which has been frequently adopted in previous simulation studies on IL/MOF composites.[7−9,19] All previous simulation studies using random model showed the improved gas uptake which has rarely been observed in experiments, implicating the impracticality of random model in simulations. The exception was observed for 1-butyl-3-methylimidazolium acetate

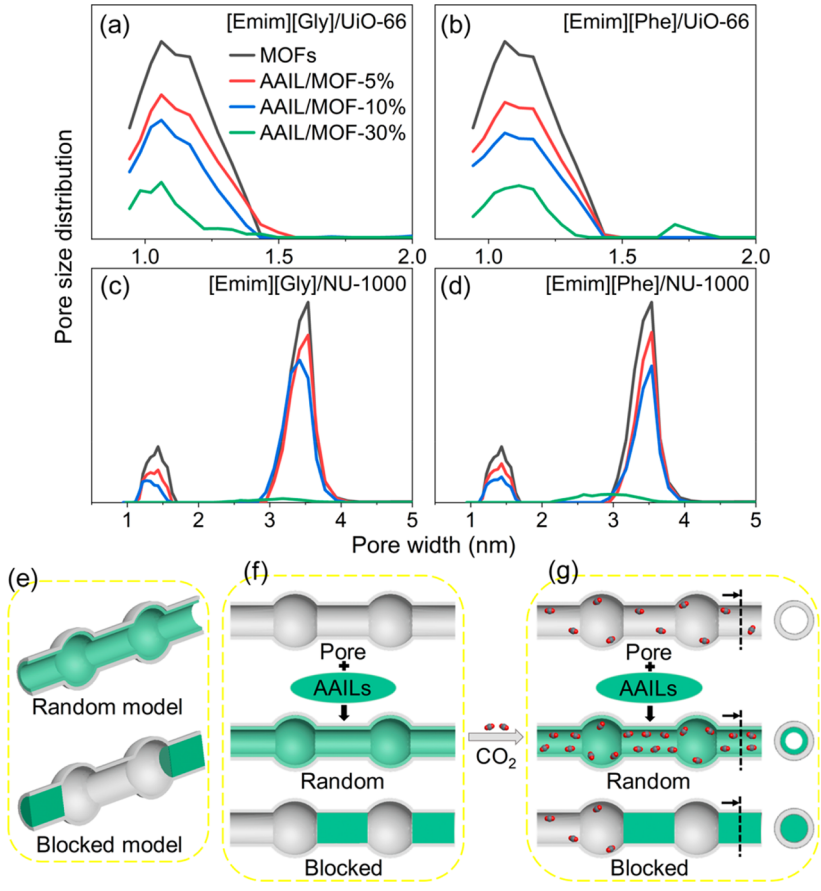

Figure 3. Pore size distribution of (a) [Emim][Gly]/UiO-66, (b) [Emim][Phe]/UiO-66, (c) [Emim][Gly]/NU-1000, and (d) [Emim][Phe]/NU-1000. (e–f) Schematic illustration of random and blocked models (f) before and (g) after CO_2 adsorption.

DOI: 10.1021/acsanm.9b01538
ACS Appl. Nano Mater. 2019, 2, 6022−6029

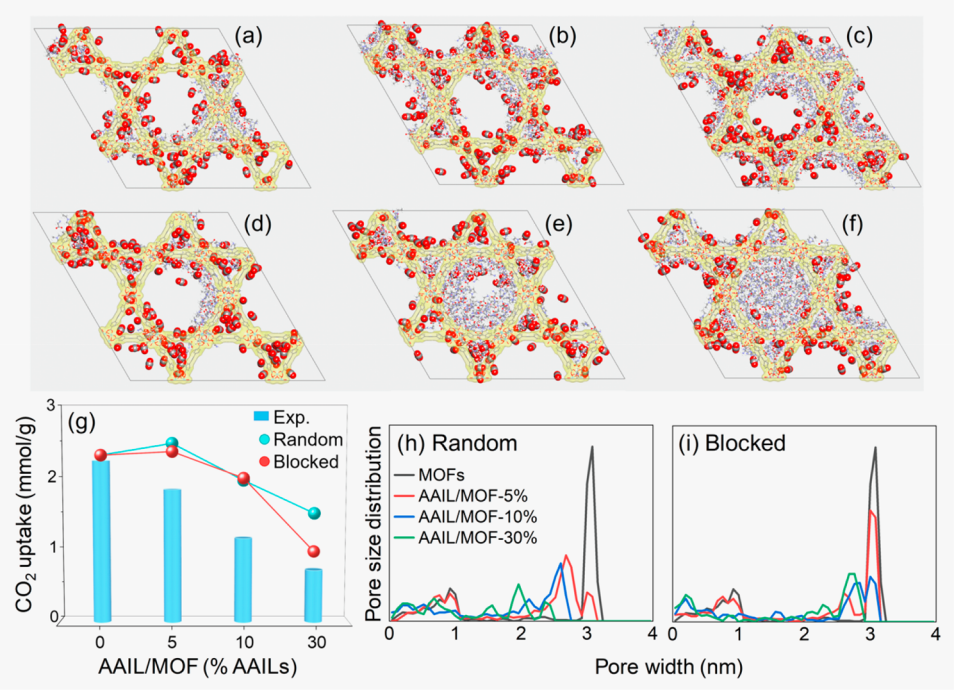

Figure 4. Snapshots of (a–c) random and (d–f) blocked models consisting of [Emim][Gly]/NU-1000 composites loaded with (a, d) 5 vol %, (b, e) 10 vol %, and (c, f) 30 vol % ILs. (g) CO_2 uptake of [Emim][Gly]/NU-1000 composites with different AAILs loadings at 298 K and 1 bar from experiment (column), random model (red symbol), and blocked model (blue symbol). (h, i) Pore size distributions of NU-1000 (black line), [Emim][Gly]/NU-1000-5% (red line), [Emim][Gly]/NU-1000-10% (blue line), and [Emim][Gly]/NU-1000-30% (green line) from (h) random model and (i) blocked model.

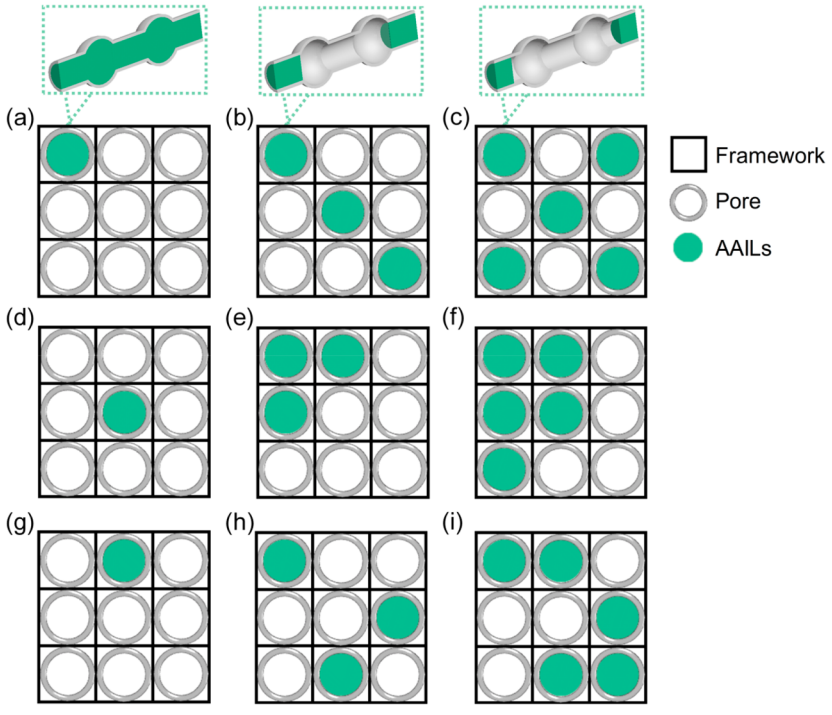

Figure 5. Schematic illustration of various possible blockage resulting from AAILs inside MOFs assuming the same amount of AAILs is loaded: (a, d, g) a single channel that was completely blocked by ILs with varying distributions in supercell of MOFs; (b, e, h) three blocked channels that were partially filled by ILs with varying distributions in supercell of MOFs; (c, f, i) five blocked channels that were partially filled by ILs with varying distributions in supercell of MOFs.

([Bmim][Ac])/ZIF-8 and1-ethyl-3-methylimidazolium acetate ([Emim][Ac])/ZIF-8 composites,[20] implicating that the tendency may depend on the type of ILs, MOFs, and IL/MOF combinations. According to our former observations of this work, there is a high possibility that pore channels have been blocked by the accumulated AAILs. Therefore, the

DOI: 10.1021/acsanm.9b01538
ACS Appl. Nano Mater. 2019, 2, 6022–6029

Scheme 1. Synthesis Process of the IL/MOF Composites

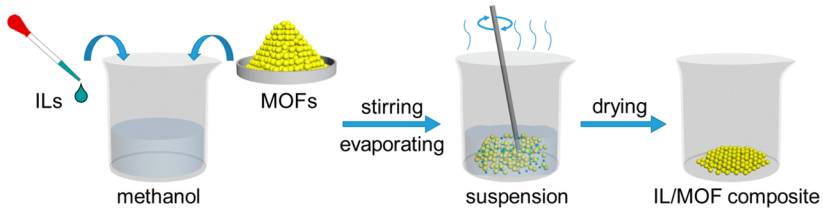

blocked model was employed for comparison (Figure 4d–f), in which AAILs assemble into specific sites of channels, thus impeding the adsorption of CO_2 molecules. Three different volume ratios of [Emim][Gly] in NU-1000 (5 vol %, 10 vol %, and 30 vol %) were taken into account in simulations, and their CO_2 uptake was presented in Figure 4g.

In general, the predicted CO_2 uptake of bare NU-1000 from simulations is in good agreement with experimental result. In contrast, upon loading AAILs, simulations using both random and blocked models give rise to the higher CO_2 uptakes than experimental measurement. With the increase of AAILs loadings, the discrepancy between the results of random and blocked models becomes significant. Specifically, random model shows the higher CO_2 uptake than the blocked model, especially at high loading (i.e., 30 vol %). At 5 vol % loading, only one small triangle pore of NU-1000 can be filled due to the small amount of ionic liquids in blocked model. Thus, only a slightly higher CO_2 uptake was observed in random model than blocked models, both of which give rise to the higher CO_2 uptake than pristine NU-1000. At 10 vol % loading, all small triangle pores of NU-1000 and a majority of the central large pores were occupied for blocked model, thus resulting in similar uptakes with that from random model. While at 30 vol % loading, the fully occupied large pore of NU-1000 leads to the remarkably lower CO_2 uptake than the random model. Compared with the random model, CO_2 uptake predicted by blocked model is closer to experimental results, verifying the existing blockage in MOFs and suggesting that the blocked model can more accurately describe the adsorption properties of IL/MOF composites. In addition, the pore size distributions of the blocked model (Figure 4i) agree better with experimental results compared with those of the random model (Figure 4h), implicating the reliability of the blocked model.

It should be noted that in practice there are numerous possibilities for the blocked channels (Figure 5). Given the limitations of computational cost, only a $2 \times 2 \times 2$ supercell of NU-1000 is established in molecular simulations. However, in experiments, the MOF crystal particle is a large supercell consisting of a large number of unit cells. Therefore, the difference in the MOF structure between simulation and experiment and the uncertainty in the detailed distributions of ILs for blocked model may cause the discrepancy between experimental measurement and simulations. There is also a possibility that the realistic blocked model is composed of a mixture of different types of blockages. Herein, several possibilities were provided in Figure 5 to illustrate how complicated blockage may occur in practice. It can also be found that once the blockage occurs, CO_2 uptake of composites is possibly dependent on the number of blocked channels rather than the amount of loaded ILs. Even a small number of ILs molecules may block multiple channels in case that only the entrances of the channels are blocked, leading to the inaccessibility of adsorption sites for CO_2 molecules. The more channels of MOFs that are blocked, the lower is the CO_2 uptake that can be inspected. According to the illustration above, the reduced CO_2 uptake of IL/MOF composites observed in experimental measurement that is opposite to the prediction from simulation may be ascribed to the blockage in channels of frameworks. In order to avoid such blockages in frameworks, it is essential to develop novel techniques to facilitate the uniform distribution of ILs in MOF channels, which should be intensively investigated in the future.

3. CONCLUSION

Although the enhanced CO_2 uptake has been reported in simulation studies, experimental measurement gives rise to opposite tendency. In this work, both experiment and molecular simulation were performed to explore the origination of the reduced CO_2 uptake of various AAIL/MOF composites in comparison with pristine MOFs. Two types of AAILs (i.e., [Emim][Gly] and [Emim][Phe]) were incorporated into two Zr-based MOFs (i.e., UiO-66 and NU-1000) at varying loadings. The CO_2 uptake of all IL/MOF composites was reduced upon AAILs loading, which decreased with the increase of the loading. Pore size distributions of these composites demonstrate that the typical pore widths of these composites are not evidently altered by introduced AAILs compared with pristine work, implicating the blocked channels of MOFs by incorporated ILs. However, to further illustrate such a phenomenon, a random model with ILs randomly distributed in NU-1000 and the blocked model with ILs artificially assembled in certain channel of NU-1000 were adopted in molecular simulations. Simulation results reveal that the blocked model gives rise to the CO_2 uptake that is closer to experimental results in comparison with random model, indicating its greater practicality. However, given the numerous possibilities of existing blockage in channels, the CO_2 uptake from simulations using blocked model may not exactly match experimental measurement. Therefore, given the occurrence of blockage with introduced ILs, we demonstrated that the random model that has been frequently used in molecular simulation for IL/MOF composite is not reliable for predicting CO_2 uptake. This work relates the decreased CO_2 uptake in IL/MOF composites to the channel blockage of frameworks resulting from ILs loading, which will inspire further experimental efforts on the elimination of channel blockage for IL/MOF composites by the development of novel techniques. However, it should be noted that the findings in this work may vary depending on the types of ILs, MOFs as well as IL/MOF combinations, which requires further investigation in the future.

4. METHODOLOGY

4.1. Experiments. *4.1.1. AAIL/MOF Composites Preparation.* UiO-66 and NU-1000 were synthesized according to previously

DOI: 10.1021/acsanm.9b01538
ACS Appl. Nano Mater. 2019, 2, 6022–6029

reported procedures with slight modifications.[21,22] The synthesis scheme is provided in Scheme 1. UiO-66 has the triangular micropores with the pore size of 6 Å,[23] whereas NU-1000 has the triangular micropores of approximately 12 Å and hexagonal mesopores of 31 Å.[24] The total pore volume of UiO-66 (0.987 cm^3/g) is smaller than NU-1000 (1.491 cm^3/g). Both [Emim][Gly] and [Emim][Phe] were purchased from commercial sources and used without any purification. AAIL/MOF composites were prepared according to the literature.[11] First, [Emim][Gly] and [Emim][Phe] were diluted 10 times with methanol. After that, the diluted AAILs were transferred into a beaker and 25 mL of methanol was added into the beaker. Then, dehydrated MOFs were added to the beaker. The resulting mixture was constantly stirred at 298 K for about 5 h until methanol was completely evaporated. Finally, the resulting sample was dried at 353 K for 12 h in a vacuum oven. AAIL/MOF composites with different AAILs loadings (i.e., 5%, 10%, and 30% (v/v)) were prepared based on the measured total pore volume of MOFs, respectively.

4.1.2. Instrumentation. PXRD data were collected on an Empyrean X-ray diffractometer from PANalytical B.V. The 2θ ranges from 4° to 50° as a continuous scan with a step size of 0.013 13° at room temperature. SEM images were collected on a Quanta 200 SEM instrument from Philips FEI. Prior to observations, all samples were coated with carbon under an acceleration voltage of 30 kV. TGA data were used to measure the thermal stability of all samples on a Pyris1 TGA from PerkinElmer instruments under a N_2 stream at the temperature ranging from room temperature to 800 °C with a heating rate of 10 °C/min. N_2 adsorption isotherms were measured at 77 K on Autosorb-iQ2 from Quantachrome Instruments. All samples were activated at 393 K for 24 h under vacuum before measurement. BET surface areas were determined by fitting the BET model to the collection on N_2 adsorption isotherms. The total pore volumes were calculated by the maximum uptake in N_2 adsorption isotherms at $P/P_0 = 0.995$. Pore size distribution was obtained from nonlocal density functional theory (NLDFT) model. CO_2 adsorption isotherms of each sample ranging from 10^{-3} to 1 bar were measured at 298 K on Autosorb-iQ2. All samples were activated at 393 K for 24 h under vacuum before measurement.

4.2. Molecular Simulations. *4.2.1. Force Field.* In simulations, modified Charmm-36 force field for [Emim][Gly] that has been validated in previous studies[25,26] was adopted. The atomic charges of [Emim][Gly] are shown in Table S5; however, those of NU-1000 are obtained from the DDEC6 method[27] by fitting the electrostatic surface potential computed by plane-wave density functional theory (DFT) using VASP package.[28] The Lennard-Jones (LJ) parameters of NU-1000 are acquired from universal force field (UFF)[29] as shown in Table S5. The nonbond intermolecular interactions of CO_2 with NU-1000 and [Emim][Gly] were obtained from LJ and Coulombic potentials (eq 1). The force field parameters have been validated in the former study.[24]

$$U_{ij} = 4\varepsilon_{ij}\left[\left(\frac{\sigma_{ij}}{r_{ij}}\right)^{12} - \left(\frac{\sigma_{ij}}{r_{ij}}\right)^{6}\right] + \frac{q_i q_j}{4\pi\varepsilon_0 r_{ij}} \quad (1)$$

i or j is the interacting particle. ε_{ij} and $\sigma_{ij}$are LJ parameters (Table S5). ε_{ij} is the depth of the well potential, and σ_{ij} is van der Waals distance. r_{ij} was the distance of two particles. q_i and q_j are the partial charges on the two interaction particles. The LJ parameters and partial charges of CO_2 are obtained from transferable potentials for phase equilibria (TraPPE)[30] force field (Table S6). The Ewald method was applied for the electrostatic interaction with a cutoff of 12.8 Å. The LJ interactions between two particles were computed using Lorentz–Berthelot mixing rule.

4.2.2. Simulation Details. A 2 × 2 × 2 MOF supercell was constructed for simulations as shown in Figure S9. Two types of [Emim][Gly]/NU-1000 composite models were built by randomly distributing [Emim][Gly] into NU-1000 (random model) and artificially blocking the pores (blocked model), respectively. Similar to previous work,[9,19,31] the random model was obtained by randomly inserting different amounts of [Emim][Gly] (5%, 10%, and 30% (v/v)) according to the available pore volume of NU-1000. The molecular volumes of ion pairs of [Emim][Gly] were calculated using the molinspiration.[32−34] Regarding the blocked model, the identical number of [Emim][Gly] molecules of random model were intentionally inserted by blocking the specific pores of MOFs. For the [Emim][Gly]/NU-1000 composite containing 5% (v/v) [Emim]-[Gly], [Emim][Gly] was preferred to fill the small pores and the remaining was located in the mesopores. For the composites containing 10% and 30% [Emim][Gly], a vast number of [Emim]-[Gly] molecules were located in the mesopores after saturating the small triangular pores of NU-1000. It is worth mentioning that the equilibrated number density of [Emim][Gly] across the mesopore of NU-1000 at 30% (v/v) loading is identical to bulk ionic liquid calculated in the same condition (Figure S10).

The [Emim][Gly]/NU-1000 composite models were initially equilibrated in a canonical (*NVT*) ensemble by MD simulation at 298 K for 10 ns in Gromacs 4.6.7. The electrostatic and van der Waals interactions were calculated with a cutoff radius of 1.3 nm, and particle-mesh Ewald method using fourth-order (cubic) interpolation[35] was used for electrostatic interaction. The integral was achieved on the equations of motion by means of Leapfrog algorithm with a time step of 1 ps.[36] Velocity-rescaled Berendsen thermostat[37] with a thermal bath time constant of 1 ps was applied. Throughout the simulations, all framework atoms were completely frozen. After obtaining the equilibrated [Emim][Gly]/NU-1000 composites from MD simulation, grand canonical Monte Carlo (GCMC) simulations of CO_2 adsorption performance of all the composites were performed at 298 K and 1 bar by RASPA version 1.9.[38] 1×10^5 MC cycles consist of 5×10^4 cycles for equilibration and 5×10^4 cycles for production run. Four Monte Carlo moves including random insertion, deletion, translation, and rotation were carried out with equal probability.

■ ASSOCIATED CONTENT

Supporting Information

The Supporting Information is available free of charge on the ACS Publications website at DOI: 10.1021/acsanm.9b01538.

Experimental details, power X-ray diffraction (PXRD), scanning electron microscope (SEM) images, thermal gravimetric analysis (TGA), adsorption and desorption isotherms, BET surface area and total pore volume, structures, Lennard-Jones (LJ) parameters, and number density (PDF)

■ AUTHOR INFORMATION

Corresponding Author

*E-mail: songli@hust.edu.cn.

ORCID

Xiaoxiao Xia: 0000-0001-9001-3662

Wei Li: 0000-0002-3920-3863

Song Li: 0000-0003-3552-3250

Author Contributions

The manuscript was written through contributions of all authors. All authors have given approval to the final version of the manuscript.

Funding

This work was funded by the National Natural Science Foundation of China (NSFC) under Project 51606081 and Double First-Class Research Funding of China-EU Institute for Clean and Renewable Energy (Grant ICARE-RP-2018-HYDRO-001). We thank the support from Analytical & Testing Center of Huazhong University of Science and Technology, and the National Supercomputer Center of Shenzhen.

DOI: 10.1021/acsanm.9b01538
ACS Appl. Nano Mater. 2019, 2, 6022−6029

Notes

The authors declare no competing financial interest.

■ ACKNOWLEDGMENTS

This work was carried out at National Supercomputer Center in Shenzhen. We thank Huazhong University of Science and Technology Analytical & Testing Center for providing support on materials characterizations.

■ ABBREVIATIONS

UiO = Universitetet i Oslo
NU = Northwestern University
IRMOF = isoreticular metal−organic framework
TDPAT = 2,4,6-tris(3,5-dicarboxylphenylamino)-1,3,5-triazine
BTC = benzene-1,3,5-tricarboxylate
ZIF = zeolitic imidazolate framework
Tf_2N = bis(trifluoromethylsulfonyl)imide
TFSA = bis(trifluoromethylsulfonyl)amide
C_3NH_2BIM = *n*-aminopropyl-3-butylimidazolium
NH_2 = amino
MIL = Matériaux de l'Institut Lavoisier
Zr = zirconium
DDEC = density derived electrostatic and chemical
VASP = Vienna ab initio simulation package

■ REFERENCES

(1) Zhou, H. C.; Kitagawa, S. Metal-Organic Frameworks (MOFs). *Chem. Soc. Rev.* **2014**, *43* (16), 5415−5418.
(2) Sumida, K.; Rogow, D. L.; Mason, J. A.; McDonald, T. M.; Bloch, E. D.; Herm, Z. R.; Bae, T. H.; Long, J. R. Carbon Dioxide Capture in Metal-Organic Frameworks. *Chem. Rev.* **2012**, *112* (2), 724−781.
(3) Yu, J.; Xie, L. H.; Li, J. R.; Ma, Y.; Seminario, J. M.; Balbuena, P. B. CO_2 Capture and Separations Using MOFs: Computational and Experimental Studies. *Chem. Rev.* **2017**, *117* (14), 9674−9754.
(4) Wang, Z.; Cohen, S. M. Postsynthetic Modification of Metal-Organic Frameworks. *Chem. Soc. Rev.* **2009**, *38* (5), 1315−1329.
(5) Lei, Z.; Chen, B.; Koo, Y. M.; MacFarlane, D. R. Introduction: Ionic Liquids. *Chem. Rev.* **2017**, *117* (10), 6633−6635.
(6) Kinik, F. P.; Uzun, A.; Keskin, S. Ionic Liquid/Metal-Organic Framework Composites: From Synthesis to Applications. *ChemSusChem* **2017**, *10* (14), 2842−2863.
(7) Chen, Y.; Hu, Z.; Gupta, K. M.; Jiang, J. Ionic Liquid/Metal-Organic Framework Composite for CO_2 Capture: A Computational Investigation. *J. Phys. Chem. C* **2011**, *115* (44), 21736−21742.
(8) Vicent-Luna, J. M.; Gutiérrez-Sevillano, J. J.; Anta, J. A.; Calero, S. Effect of Room-Temperature Ionic Liquids on CO_2 Separation by a Cu-BTC Metal-Organic Framework. *J. Phys. Chem. C* **2013**, *117* (40), 20762−20768.
(9) Li, Z.; Xiao, Y.; Xue, W.; Yang, Q.; Zhong, C. Ionic Liquid/Metal-Organic Framework Composites for H_2S Removal from Natural Gas: A Computational Exploration. *J. Phys. Chem. C* **2015**, *119* (7), 3674−3683.
(10) Silva, F. W. M. d.; Magalhães, G. M.; Jardim, E. O.; Silvestre-Albero, J.; Sepúlveda-Escribano, A.; de Azevedo, D. C. S.; de Lucena, S. M. P. CO_2 Adsorption on Ionic Liquid-Modified Cu-BTC: Experimental and Simulation Study. *Adsorpt. Sci. Technol.* **2015**, *33* (2), 223−242.
(11) Sezginel, K. B.; Keskin, S.; Uzun, A. Tuning the Gas Separation Performance of CuBTC by Ionic Liquid Incorporation. *Langmuir* **2016**, *32* (4), 1139−1147.
(12) Ma, J.; Ying, Y.; Guo, X.; Huang, H.; Liu, D.; Zhong, C. Fabrication of Mixed-Matrix Membrane Containing Metal-Organic Framework Composite with Task-Specific Ionic Liquid for Efficient CO_2 Separation. *J. Mater. Chem. A* **2016**, *4* (19), 7281−7288.
(13) Ban, Y.; Li, Z.; Li, Y.; Peng, Y.; Jin, H.; Jiao, W.; Guo, A.; Wang, P.; Yang, Q.; Zhong, C.; Yang, W. Confinement of Ionic Liquids in Nanocages: Tailoring the Molecular Sieving Properties of ZIF-8 for Membrane-Based CO_2 Capture. *Angew. Chem., Int. Ed.* **2015**, *54* (51), 15483−15487.
(14) Kinik, F. P.; Altintas, C.; Balci, V.; Koyuturk, B.; Uzun, A.; Keskin, S. [BMIM][PF_6] Incorporation Doubles CO_2 Selectivity of ZIF-8: Elucidation of Interactions and Their Consequences on Performance. *ACS Appl. Mater. Interfaces* **2016**, *8* (45), 30992−31005.
(15) Koyuturk, B.; Altintas, C.; Kinik, F. P.; Keskin, S.; Uzun, A. Improving Gas Separation Performance of ZIF-8 by [BMIM][BF_4] Incorporation: Interactions and Their Consequences on Performance. *J. Phys. Chem. C* **2017**, *121* (19), 10370−10381.
(16) Bai, Y.; Dou, Y.; Xie, L. H.; Rutledge, W.; Li, J. R.; Zhou, H. C. Zr-Based Metal-Organic Frameworks: Design, Synthesis, Structure, and Applications. *Chem. Soc. Rev.* **2016**, *45* (8), 2327−2367.
(17) Fukumoto, K.; Yoshizawa, M.; Ohno, H. Room Temperature Ionic Liquids from 20 Natural Amino Acids. *J. Am. Chem. Soc.* **2005**, *127* (8), 2398−2399.
(18) Fujie, K.; Yamada, T.; Ikeda, R.; Kitagawa, H. Introduction of an Ionic Liquid into the Micropores of a Metal-Organic Framework and Its Anomalous Phase Behavior. *Angew. Chem., Int. Ed.* **2014**, *53* (42), 11302−11305.
(19) Gupta, K. M.; Chen, Y.; Jiang, J. Ionic Liquid Membranes Supported by Hydrophobic and Hydrophilic Metal-Organic Frameworks for CO_2 Capture. *J. Phys. Chem. C* **2013**, *117* (11), 5792−5799.
(20) Mohamedali, M.; Ibrahim, H.; Henni, A. Incorporation of Acetate-Based Ionic Liquids into a Zeolitic Imidazolate Framework (ZIF-8) as Efficient Sorbents for Carbon Dioxide Capture. *Chem. Eng. J.* **2018**, *334*, 817−828.
(21) Schaate, A.; Roy, P.; Godt, A.; Lippke, J.; Waltz, F.; Wiebcke, M.; Behrens, P. Modulated Synthesis of Zr-Based Metal-Organic Frameworks: From Nano to Single Crystals. *Chem. -Eur. J.* **2011**, *17* (24), 6643−6651.
(22) Wang, T. C.; Vermeulen, N. A.; Kim, I. S.; Martinson, A. B.; Stoddart, J. F.; Hupp, J. T.; Farha, O. K. Scalable Synthesis and Post-Modification of a Mesoporous Metal-Organic Framework Called NU-1000. *Nat. Protoc.* **2016**, *11* (1), 149−162.
(23) Cavka, J. H.; Jakobsen, S.; Olsbye, U.; Guillou, N.; Lamberti, C.; Bordiga, S.; Lillerud, K. P. A New Zirconium Inorganic Building Brick Forming Metal Organic Frameworks with Exceptional Stability. *J. Am. Chem. Soc.* **2008**, *130* (42), 13850−13851.
(24) Deria, P.; Mondloch, J. E.; Tylianakis, E.; Ghosh, P.; Bury, W.; Snurr, R. Q.; Hupp, J. T.; Farha, O. K. Perfluoroalkane Functionalization of NU-1000 via Solvent-Assisted Ligand Incorporation: Synthesis and CO_2 Adsorption Studies. *J. Am. Chem. Soc.* **2013**, *135* (45), 16801−16804.
(25) Fileti, E. E.; Chaban, V. V. The Force Field for Imidazolium-Based Ionic Liquids: Novel Anions with Polar Residues. *Chem. Phys. Lett.* **2015**, *633* (1), 132−138.
(26) Fileti, E. E.; Chaban, V. V. The Scaled-Charge Additive Force Field for Amino Acid Based Ionic Liquids. *Chem. Phys. Lett.* **2014**, *616−617*, 205−211.
(27) Manz, T. A.; Limas, N. G. Introducing DDEC6 Atomic Population Analysis: Part 1. Charge Partitioning Theory and Methodology. *RSC Adv.* **2016**, *6* (53), 47771−47801.
(28) Hafner, J. Ab-Initio Simulations of Materials Using VASP: Density-Functional Theory and Beyond. *J. Comput. Chem.* **2008**, *29* (13), 2044−2078.
(29) Rappe, A. K.; Casewit, C. J.; Colwell, K. S.; Goddard, W. A., III; Skiff, W. M. UFF, a Full Periodic Table Force Field for Molecular Mechanics and Molecular Dynamics Simulations. *J. Am. Chem. Soc.* **1992**, *114* (25), 10024−10035.
(30) Potoff, J. J.; Siepmann, J. I. Vapor-Liquid Equilibria of Mixtures Containing Alkanes, Carbon Dioxide, and Nitrogen. *AIChE J.* **2001**, *47* (7), 1676−1682.
(31) Gupta, K. M.; Chen, Y.; Hu, Z.; Jiang, J. Metal-Organic Framework Supported Ionic Liquid Membranes for CO_2 Capture: Anion Effects. *Phys. Chem. Chem. Phys.* **2012**, *14* (16), 5785−5794.

DOI: 10.1021/acsanm.9b01538
ACS Appl. Nano Mater. 2019, 2, 6022−6029

(32) Ertl, P.; Rohde, B.; Selzer, P. Fast Calculation of Molecular Polar Surface Area as a Sum of Fragment-Based Contributions and Its Application to the Prediction of Drug Transport Properties. *J. Med. Chem.* **2000**, *43* (20), 3714−3717.
(33) Lipinski, C. A.; Lombardo, F.; Dominy, B. W.; Feeney, P. J. Experimental and Computational Approaches to Estimate Solubility and Permeability in Drug Discovery and Development Settings. *Adv. Drug Delivery Rev.* **2001**, *46* (1−3), 3−26.
(34) Veber, D. F.; Johnson, S. R.; Cheng, H. Y.; Smith, B. R.; Ward, K. W.; Kopple, K. D. Molecular Properties That Influence the Oral Bioavailability of Drug Candidates. *J. Med. Chem.* **2002**, *45* (12), 2615.
(35) Darden, T.; York, D.; Pedersen, L. Particle Mesh Ewald: An N-log(N) Method for Ewald Sums in Large Systems. *J. Chem. Phys.* **1993**, *98* (12), 10089−10092.
(36) Hockney, R. W. The Potential Calculation and Some Applications. In *Methods in Computational Physics. IX. Plasma Physics*; Academic: London, U.K., 1970; pp 135−211.
(37) Berendsen, H. J. C.; Postma, J. P. M.; van Gunsteren, W. F.; DiNola, A.; Haak, J. R. Molecular Dynamics with Coupling to an External Bath. *J. Chem. Phys.* **1984**, *81* (8), 3684−3690.
(38) Dubbeldam, D.; Calero, S.; Ellis, D. E.; Snurr, R. Q. RASPA: Molecular Simulation Software for Adsorption and Diffusion in Flexible Nanoporous Materials. *Mol. Simul.* **2016**, *42* (2), 81−101.

DOI: 10.1021/acsanm.9b01538
ACS Appl. Nano Mater. 2019, 2, 6022−6029